Supplementary Information: Rhombohedral trilayer graphene being more stable than its Bernal counterpart†

R. Guerrero-Avilés,[a] M. Pelc,[a,b] F. R. Geisenhof,[c] R. T. Weitz[d] and A. Ayuela[a*]

1 Convergence Tests

Energy differences between stackings in the main text are below meV/nm^2, values that are in the typical order of magnitude for van der Waals (vdW) interactions. The total vdW interaction in a sample depends on the surface area, in the sense that a stacking is experimentally stabilized when it is above a critical area, so that the layers remain stacked and sliding is avoided; otherwise, the layers would be switching between several stackings at room temperature. Because the main text focuses on the energy differences between stackings, the computational parameters have to be well converged. We consider it necessary to asses the convergence tests in more detail than for other materials, as included here in the SI.

Crucial convergence energy tests require the analysis of cut-offs, broadening energy values, and k-meshes. However, we first ensure that the energy differences between the Bernal and rhombohedral stackings are converged within few μeVs per nm^2. The energy for each stacking in our calculations should be stable well below this energy tolerance in electronic self-consistency. We then choose the values of convergence tolerance between

[a] *Material Physics Center CFM-MPC, Donostia International Physics Center (DIPC), Paseo Manuel Lardizabal 4-5, 20018 Donostia-San Sebastián, Spain. E-mail: swxayfea@sw.ehu.es*
[b] *Institute of Physics, Nicolaus Copernicus University in Toruń, Grudziadzka 5, 87-100 Toruń, Poland.*
[c] *Physics of Nanosystems, Department of Physics, Ludwig-Maximilians-Universität München, Amalienstrasse 54, 80799 Munich, Germany.*
[d] *I. Physikalisches Institut, Friedrich-Hund-Platz 1, 37077 Göttingen, Germany.*

10^{-7}-10^{-8} eV corresponding to the electronic self-consistency, and when performing relaxations we use a force convergence criterion of 1.0 μeV/Å. These selected values guarantee that stacking energy differences in the order of tenths or even hundreds of a meV remain meaningful.

1.1 Cut-off Energy Test

We present an energy cut-off convergence test for plane wave basis, using the k-mesh set to 30×30 and the smearing value to $\sigma = 0.05$ eV. The energy differences between Bernal

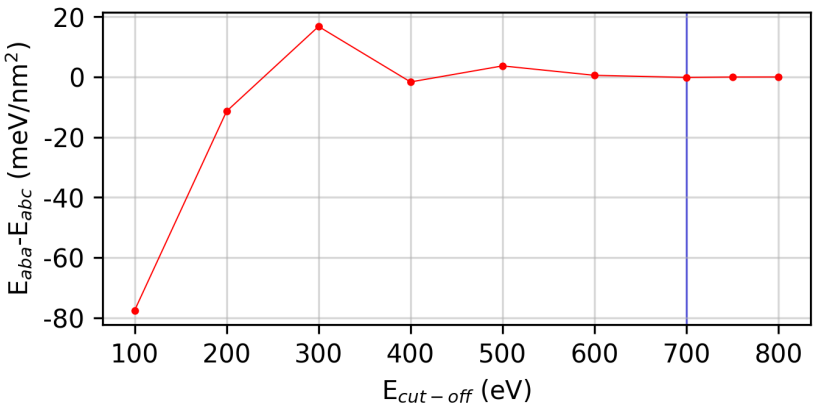

Fig. 1 Convergence test for energy differences between the Bernal and rhombohedral stacking against kinetic cut-off energies.

and rhombohedral stackings are shown in Fig 1. The blue line marks the well converged cut-off value of 700 eV chosen for the calculations. For this value, the energy difference between stackings relative to the most stable one is converged in the order of μeV per nm^2, much below the energy differences between stackings to be discussed in the main text.

1.2 Broadening Energy Test

The following energy test focuses on the σ parameter used for broadening energies in the discrete integration points of the irreducible Brillouin zone. This broadening energy test is essential, especially to describe the state occupation of electronic bands split around the Fermi level. When the σ value is too large, the smearing function is counting states from

the conduction bands as fully or partially occupied states. For large σ values, the band splitting around the Fermi energy can be overlooked by averaging. When the σ values are too small the levels are considered as if the system is studied at small temperatures. Furthermore, σ values could not be made too small because for a finite number of k points it would be like using a discrete set of levels. Then, for performing practical integrations there is a region in the middle where the optimum σ values should be selected. A test using Gaussian smearing and a k-mesh of 30×30 was presented. Figure 2 shows the stacking energy difference as a function of the σ values. The results show a region of minimum σ values, following a different trend than that obtained in the previous cutoff energy test. We choose the value of $\sigma = 10^{-2}$eV, for which the differences reach a minimum; this value is marked with the blue line. The relative energy difference between Bernal and rhombohedral stackings amounts to 904.402 μeV/nm^2. It is also noteworthy that the chosen σ value is able to discriminate the splitting between the flats bands around the K, K' points for the rhombohedral stacking [Fig 1 (a)].

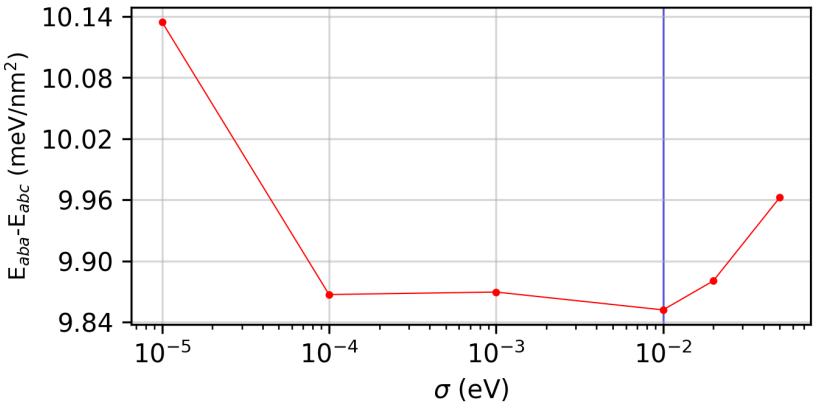

Fig. 2 Convergence test for the stacking energy difference against the broadening energy (σ) using gaussian smearing.

1.3 K-mesh Energy Test

We generated k-mesh grids centered at the Γ point for trilayer graphene as because hexagonal lattices must be treated with some subtlety[1]. In our calculations, we use a regular

grid of equidistant points in reciprocal space by using the Monkhorst-Pack sampling, and the used total number of k-points is reduced according to cell symmetries. Figure 3 shows the energy difference between the Bernal and rhombohedral stackings versus the number of k-points considered. The red curve shows the energy differences for the $k\times k$ mesh with the k number being a multiple of 3, and the gray broad curve collects the points obtained with other k meshes. The two curves show differences at a qualitative level: in the case of the gray curve the energy difference is negative for small k-mesh values, which implies that the Bernal stacking would have been obtained as the favorable one, a result that does not agree with those obtained in the red curve and the fully converged results. The red curve following the *multiples of 3 includes the high symmetry K, K' points explicitly in the k-mesh*. For our energy tolerance criteria, on the order of a few μeV per nm^2, the energy differences are stabilized for the k values of k-meshes larger than 174$\times$174. Because the Dirac cones in graphene systems are located at the K, K' points around which crucial physics is happening, omitting these points can lead to incorrect qualitative trends, specially when careful convergence in the number of k points has not been performed.

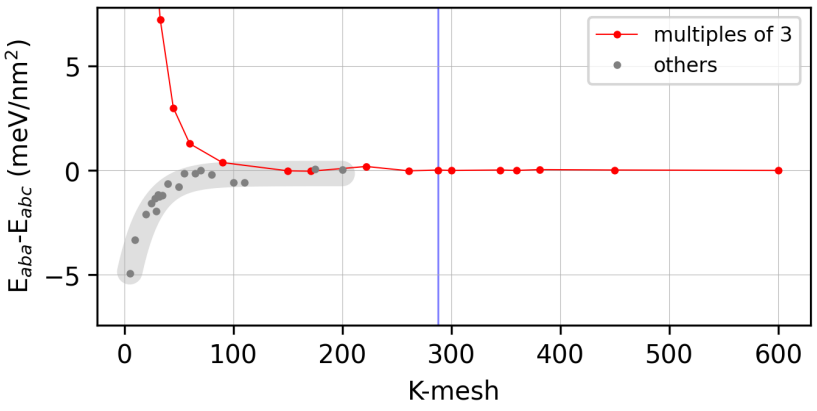

Fig. 3 Differences in stacking energies versus the number of k-points in the reciprocal mesh. The red curve corresponds to k$\times$k meshes with k being multiples of 3 and including the K, K' points; the thick gray curve collects all other cases. For the k-values larger than 174, the energy differences are converged to the required accuracy limit.

The reciprocal zone sampled with a regular set of k-points does not necessarily include

some of the high symmetry points when the TLG phases studied in the article are further deformed anisotropically. Even for the k-mesh values being multiple of 3, a regular grid does not include the high symmetry K, K' points unless k-points are commensurated in the two orthogonal directions in the plane. In those cases a very fine k point sampling is required. We are using a k-mesh of 288×288 in our calculations, marked with the blue line in Fig.3, with well-converged energies even for the cases of non-regular deformed lattices. For the mesh value of 288, the energy difference between the stackings becomes 655.691 μeV/nm^2. We perform a test to study the mismatch when taking high symmetry points or not, and we include them by hand modifying the corresponding weights. The stacking energy differences for k-meshes larger than 174 agree using the two types of k-meshes within μeV per nm^2. This comparison indicates that the bands structures for the deformed layers are well described by the chosen regular k point mesh described above.

2 Tests Using Several vdW Functionals

Different energy functionals are tested to study van der Waals interactions between layers. The parameters selected to perform DFT functional tests were the converged ones found above in Fig 1-3. Figure 4 collects the energy differences between the Bernal and rhombohedral stacking for the most common functionals that are used to study the dispersive interactions.* Functionals tested here give different relative energies but all of them favor the rhombohedral stacking. The local density approximation (LDA) within density functional theory gives us a good approach to the structural stability and vibrations in multilayer graphene-like systems. Using LDA, the rhombohedral stacking is already more stable than the Bernal by 9.44 meV/nm^2. There are vdW functionals including Grimme corrections, which are added to generalized gradient approximation (GGA) for the exchange and correlation part[2]. The Grimme correction is a semi-empirical adjustment of

* For the test we are using the following parameters: cut-off energy 700 eV, σ-energy 0.01 eV, electronic self-consistent energy tolerance 10^{-8} eV, k-mesh 30×30, and force tolerance for the relaxations of atoms and cells 10^{-7} eV/Å.

the non-local and long-range interactions. We tried two flavors of the Grimme fitting, the most common one named vdW-D2 and the damped one labelled as vdW-D3 that includes an extra term for damping[3,4]. We find that the stacking energy differences for the D2 and D3 flavours are given as 8.57 meV/nm^2 and 10.49 meV/nm^2, respectively, being the rhombohedral stacking favorable in both cases.

One of the latest approaches to study van der Waals interactions is the vdW-DF functional[5]. The nonlocal exchange-correlation energy in the electron interactions follows the expression $E_{xc}=E_x^{GGA}+E_c^{LDA}+E_c^{nl}$, where the subscripts x and c indicates exchange and correlation, and the subscript nl indicates the nonlocal contribution. Again we see that the rhombohedral stacking is the more stable phase with a relative energy difference of 9.02 meV/nm^2. Another test was performed using the vdW-DF2 functional, which is designed to be reliable for sparse systems in biological matter applications, and organic elements involved in carbonaceous systems[6–8]. The vdW-DF2 functional improves the nonlocal term of the correlation energy, and replaces the revPBE exchange term of vdW-DF functional with a PW86 term[9], because the revPBE exchange term is more repulsive[10]. The energy difference between stackings is 9.74 meV/nm^2, with the rhombohedral stacking being even more favorable. Finally we consider the rev-vdW-DF2 functional, one of the most modern functional versions of the vdW-DF family designed for inhomogeneous systems[11]. The energy difference between stackings becomes 9.64 meV/nm^2, in good agreement with all previous vdW calculations.

All the tested functionals calculate the energy differences between the Bernal and rhombohedral stacking agreeing on both trends and values. Figure 4 helps to see that other functionals used for graphene give similar trends when the accuracy is taken properly into account, so our results would be valid independently of the used functional. However, we choose the vdW-DF2 functional to present the results in the main text. As explained above the vdW-DF2 functional describes better the interactions between layers of graphene. Furthermore, other functionals within the same family seem to be overesti-

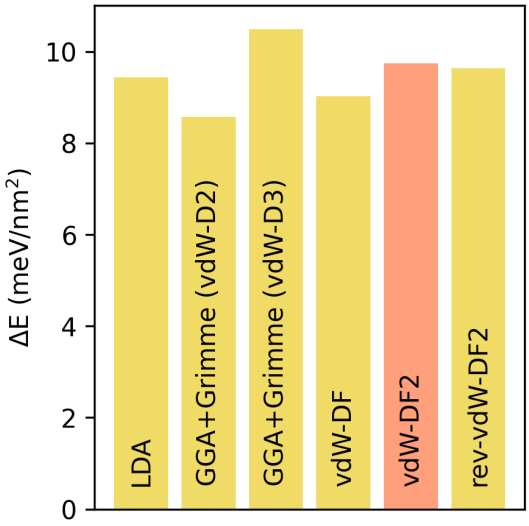

Fig. 4 Stacking energy differences ($\Delta E = E_{aba} - E_{abc}$) using several functionals to dealt with non-local dispersive interactions.

mating the interlayer distances and the binding energies[12].

There is no clear agreement on which functional has to be selected for systems like few-layer graphene because the performance of each functional is still under discussion. The functionals that best reproduce the interlayer distance have a lack of accuracy when calculating the binding energies even in pure graphite. Although many of them have acceptable performance for clusters and molecules, functional transferability is still discussed because graphene layer systems show emergent properties. For instance, systems like TGL do not behave exactly like graphite in the interlayer distances and more importantly in their electronic properties[12–14]. Independently of the functional tests made in this section, we have already validated our DF2 results obtained for the stackings of TLG in the main text with experimental results, and found that trends are in agreement as discussed in a previous work[15].

3 Farthest Shear Deformations in Stackings

Simulations of the trilayer graphene structures under shear deformations were performed for different ϕ and θ angles. The (ϕ, θ) values of the shear deformations around the Bernal

and rhombohedral stackings are given using blue and red dots, respectively, as shown in Fig. 5. The (ϕ, θ) pairs given in grey crosses denotes large deformations, so that atoms find more nearest neighbors between graphene layers and we can no longer treat shear structures as close to the Bernal and rhombohedral geometries. It is noteworthy that the limit values differ for both stackings and reveal different periodicity, namely 60° for the deformations around the Bernal stacking and 120° for those around the rhombohedral stacking. Therefore, the relative stability between stackings follows the lower periodicity of 60° as shown in the inset of Fig. 4 described in the main text.

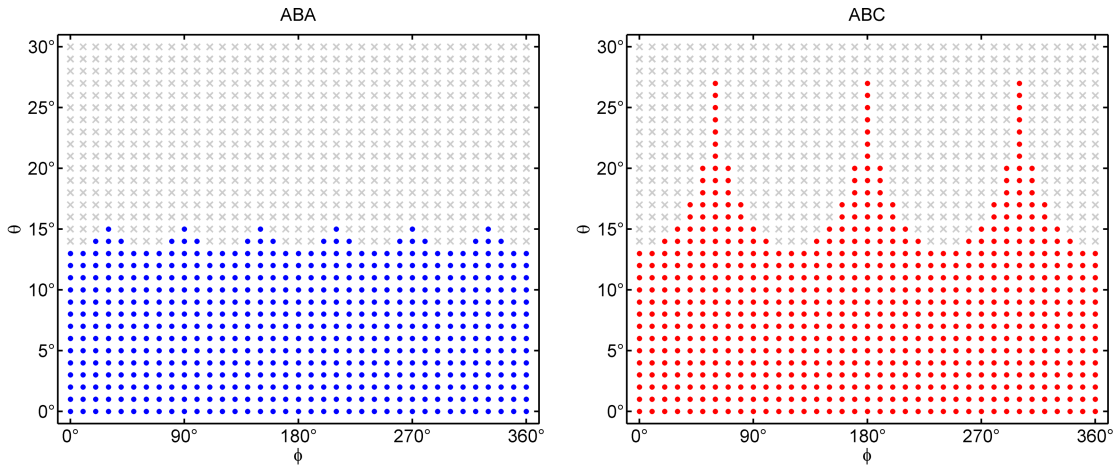

Fig. 5 Close stackings to the Bernal and rhombohedral geometry under shear deformation. Dots refer to the values of θ and ϕ angles for which the stacking geometry is nearly preserved, crosses when we no longer can call these geometries Bernal and rhombohedral.

3.1 Rhombohedral Trilayer Graphene Stacking under Shear: Electronic Spectrum

In our study we applied shear to rhombohedral and Bernal stackings and examine their relative energies as shown in Sec.5 of the main text. Here we analyze the changes in band structure for the rhombohedral case because its change in energy is large. This study is related to how lattice distortions could affect van Hove singularities. Figure 6 shows the band structures of rhombohedral trilayer graphene for a shear of θ=5° and ϕ=0°. In the undistorted case, the bands around the K, K′ points have electron-hole symmetry near the Fermi energy and in the following bands around $\pm$0.25 eV, labeled here as primary

and secondary subbands, respectively. However, the electron-hole symmetry is lost under shear. Here, the bands of the path line ΓK shift down in energy, and those along the path KM move to left in energy with bands almost crossing at the K point.

In the undistorted case, the primary and secondary subbands have different origins. The secondary bands came from the hybridization of nearest-neighbors sites between layers[16]. The primary bands come from uncoupled outerlayers nodes (over middle layer hollows); these bands induce flat regions at the K K′ points, which are related to the van Hove singularities at the Fermi energy. With shear, the secondary bands change directly because the coupling between layers is modified by tilting. Thus, the corresponding van Hove singularities are expected to split.

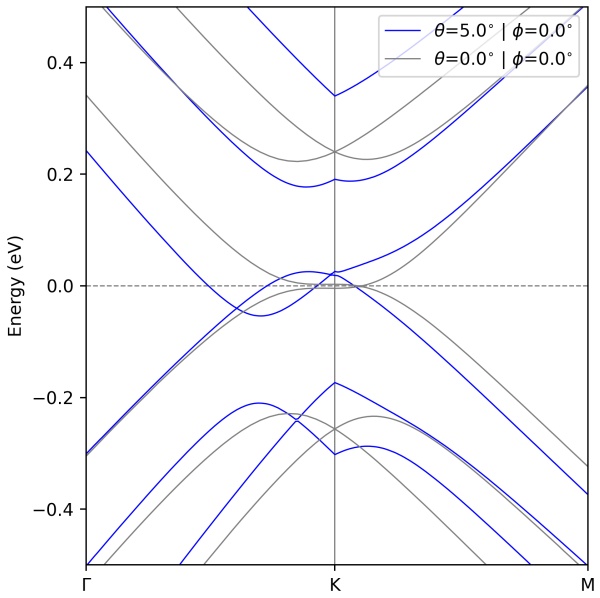

Fig. 6 Electronic band structure for pristine and sheared rhombohedral trilayer graphene. Spectrum plotted around the K K′ points along the $\Gamma - K - M$ path.

Concerning the primary bands, the outer sublattices enhance their coupling with the middle layer due to shear; this provokes that these bands redistribute the charge at the Fermi level with respect to the unrelaxed case. In fact, the Fermi level of the layers with shear cross the bands at several points, moving charge for a part to other around the K valley. This finding suggests a charge transfer in the unconnected nodes of outer layers

so that van Hove singularities are moved away from the Fermi energy. Additionally, this charge redistribution matches with the translation along the KM path line bands. This energy shift and translation can be explained by an interlayer 1D pattern, which a reasonable assumption assuming how the shear distortion breaks the symmetry around carbon atoms, a detailed study which is beyond the actual scope of this paper.

References

1 G. Kresse and J. Hafner, *Phys. Rev. B*, 1993, **47**, 558–561.

2 S. Grimme, *J. Comput. Chem.*, 2006, **27**, 1787–1799.

3 S. Grimme, J. Antony, S. Ehrlich and H. Krieg, *J. Chem. Phys.*, 2010, **132**, 154104.

4 S. Grimme, S. Ehrlich and L. Goerigk, *J. Comput. Chem.*, 2011, **32**, 1456–1465.

5 M. Dion, H. Rydberg, E. Schröder, D. C. Langreth and B. I. Lundqvist, *Phys. Rev. Lett.*, 2004, **92**, 246401–246404.

6 K. Lee, E. D. Murray, L. Kong, B. I. Lundqvist and D. C. Langreth, *Phys. Rev. B*, 2010, **82**, 081101–081104.

7 G. Román-Pérez and J. M. Soler, *Phys. Rev. Lett.*, 2009, **103**, 096102.

8 J. Klimeš, D. R. Bowler and A. Michaelides, *Phys. Rev. B*, 2011, **83**, 195131.

9 J. P. Perdew and W. Yue, *Phys. Rev. B*, 1986, **33**, 8800–8802.

10 Y. Zhang and W. Yang, *Phys. Rev. Lett.*, 1998, **80**, 890.

11 I. Hamada, *Phys. Rev. B*, 2014, **89**, 121103–121107.

12 I. V. Lebedeva, A. V. Lebedev, A. M. Popov and A. A. Knizhnik, *Comput. Mater. Sci.*, 2017, **128**, 45–58.

13 F. Tran, L. Kalantari, B. Traoré, X. Rocquefelte and P. Blaha, *Phys. Rev. Mater.*, 2019, **3**, 063602–063617.

14 T. Björkman, *J. Chem. Phys.*, 2014, **141**, 074708–074713.

15 F. R. Geisenhof, F. Winterer, S. Wakolbinger, T. D. Gokus, Y. C. Durmaz, D. Priesack, J. Lenz, F. Keilmann, K. Watanabe, T. Taniguchi, R. Guerrero-Avilés, M. Pelc, A. Ayuela and R. T. Weitz, *ACS Appl. Nano Mater.*, 2019, **2**, 6067–6075.

16 S. Xu, M. M. Al Ezzi, N. Balakrishnan, A. Garcia-Ruiz, B. Tsim, C. Mullan, J. Barrier, N. Xin, B. A. Piot, T. Taniguchi, K. Watanabe, A. Carvalho, A. Mishchenko, A. K. Geim, V. I. Fal'ko, S. Adam, A. H. C. Neto, K. S. Novoselov and Y. Shi, *Nat. Phys.*, 2021, **17**, 619–626.